We are IntechOpen, the world's leading publisher of Open Access books Built by scientists, for scientists

4,800
Open access books available

122,000
International authors and editors

135M
Downloads

Our authors are among the

154
Countries delivered to

TOP 1%
most cited scientists

12.2%
Contributors from top 500 universities

CLARIVATE ANALYTICS BOOK CITATION INDEX INDEXED

WEB OF SCIENCE™

Selection of our books indexed in the Book Citation Index in Web of Science™ Core Collection (BKCI)

Interested in publishing with us?
Contact book.department@intechopen.com

Numbers displayed above are based on latest data collected.
For more information visit www.intechopen.com

Chapter 13

First-Transition Metal Oxocomplex–Surface-Modified Titanium(IV) Oxide for Solar Environmental Purification

Hiroaki Tada and Qiliang Jin

Additional information is available at the end of the chapter

http://dx.doi.org/10.5772/62008

Abstract

The ongoing global energy and environmental issues warrant the development of environmental catalysts for decomposing pollutants in water and air by utilizing solar energy named as "solar environmental catalysts." This chapter describes the recent studies on a novel class of solar environmental catalysts consisting of TiO_2 and molecular-scale first-row transition metal oxide clusters (or metal oxocomplexes) on the surface (MOs/TiO_2). The TiO_2 surface modification with the oxocomplexes by the chemisorption–calcination cycle (CCC) technique presents a novel band engineering for fine-tuning the band energy. The unique physicochemical and electronic properties of MOs/TiO_2 give rise to the outstanding photocatalytic activity for the decomposition of organic pollutants. The combination with the rapidly growing technique for preparation of TiO_2 nanostructures allows us to expect further improvement of the performances and the wide application to the solar chemical transformation for producing useful substances.

Keywords: Visible-light photocatalyst, Titanium(IV) oxide, Surface modification, Metal oxide cluster, Metal oxocomplex, Band energy turning, Solar environmental purification

1. Introduction

Environmental pollution is beyond limits, and the development of environmental catalysts is a critical subject for scientists and engineers all over the world. Here, the catalysts for purifying polluted water and air by utilizing the solar energy are termed as "solar environmental catalyst." The TiO_2 photocatalyst possesses great potential as the "solar environmental catalyst" owing to its strong oxidation ability, high physicochemical stability, abundance in nature, and nontoxicity [1,2]. Scheme 1 shows the fundamental reaction mechanism on the TiO_2-photocatalyzed decomposition of organic pollutants with the characteristic time for each process [3]. UV-light absorption by TiO_2 causes the excitation of electrons in the valence band (VB) to the

conduction band (CB) in the order of femtoseconds. Most of the photogenerated charge carriers are lost by the recombination within ~100 ns. The charge carriers surviving the recombination are trapped at the TiO_2 surface to induce the redox reactions. In general, the CB electrons reduce oxygen (O_2), whereas the VB holes oxidize organic pollutants. The VB holes have a highly positive potential (+2.67 V versus standard hydrogen electrode (SHE) at pH 7) to oxidize most organic compounds. Conversely, the driving force for one-electron O_2 reduction (standard potential, $E^0(O_2/O_2^-)$ = −0.284 V versus SHE) by the CB electrons (−0.53 V versus SHE at pH 7) is small. Consequently, the O_2 reduction reaction (ORR) is much slower (~ms) than the oxidation process (~100 ns). TiO_2 usually takes crystal forms of rutile and anatase. The flatband potential of anatase is ~0.2 V, which is more negative than that of rutile, and anatase has a higher UV-light activity for the oxidation of organic compounds as compared with rutile [4]. This fact also points to the importance of the ORR in TiO_2 photocatalytic reactions. Also, the coupling of anatase and rutile TiO_2 can further increase the UV-light activity because of the enhancement of charge separation due to the interfacial electron transfer [5].

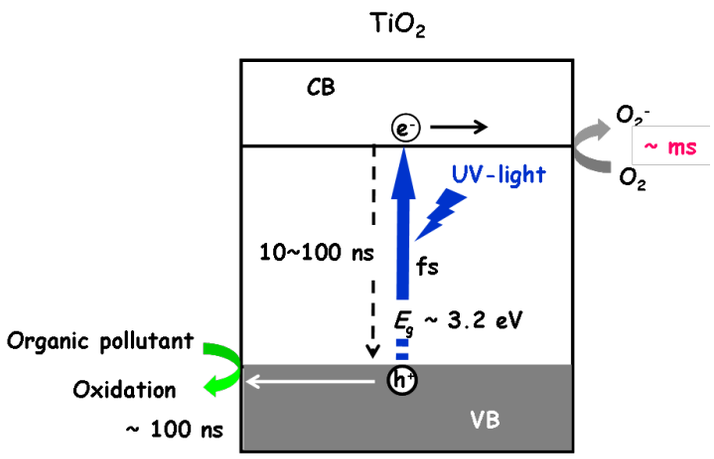

Sheme 1. The basic mechanism on the TiO_2 photocatalytic reaction (the surface trapping processes for the CB electrons and VB holes are abbreviated) with the characteristic time for each step shown.

Recently, the visible-light activation of TiO_2 by its surface modification with metal oxide nanoparticles (NPs) or oxocomplexes has been developed [6,7]. This approach has a major advantage over the conventional doping [8–14], in that visible-light activation can be achieved by a simple procedure without the introduction of the impurity/vacancy levels into the bulk TiO_2. To date, the impregnation method has been mainly used for the surface modification with metal oxide NPs, including chromium oxides [15], iron oxides [16–18], and copper oxides [19]. Unfortunately, the surface modification by the impregnation method is effective for rutile but less effective for anatase.

This chapter deals with our recent studies on the surface modification of anatase TiO_2 with the first (3d) transition metal oxocomplexes (MOCs) by the chemisorption–calcination cycle technique (MOCs/TiO_2) [20] and the characterization and photocatalytic activities for the degradation of organic pollutants. We show that some MOCs/TiO_2 fulfill the requirements for the "solar environmental catalyst."

http://dx.doi.org/10.5772/62008

2. Design for solar environmental catalysts

The requirements for the highly active TiO_2-based "solar environmental catalyst" are described below. As shown in Figure 1, the excitation from the VB electrons to the CB needs UV-light irradiation, occupying only 3% of the incident sunlight. From a viewpoint of the effective use of the sunlight, the response to the visible-light occupying 45% of the solar energy (Figure 1) should be particularly imparted to anatase TiO_2 and anatase–rutile-mixed TiO_2 (Requirement 1). However, even if TiO_2 can be endowed with the visible-light activity, it is usually much smaller than the UV-light activity. Therefore, the inherent excellent UV-light activity of TiO_2 should be compatible with the visible-light activity (Requirement 2). For high levels of visible and UV-light activities to be achieved, the enhancement of the ORR is crucial because it is usually the rate-determining step in the TiO_2-photocatalyzed reactions [21] (Requirement 3).

3. Catalyst preparation

3.1. Chemisorption–calcination cycle technique

The adsorption mechanism of metal acetylacetonates (acac) on TiO_2 depends on the kind of complexes. As an example, Fe oxocomplex formation by the CCC technique is represented in Scheme 2. In the first step, $Fe(acac)_3$ is chemisorbed on the TiO_2 surface via the ligand exchange between the acac ligand and the surface Ti-OH group from the nonaqueous solution (Eq. 1) [22]:

$$Fe(acac)_3 + l(Ti_s\text{-}OH) \rightarrow Fe(acac)_{3-l}(O\text{-}Ti_s)_l + lAcacH \quad (l \approx 1) \tag{1}$$

where the subscript s denotes the surface atom.

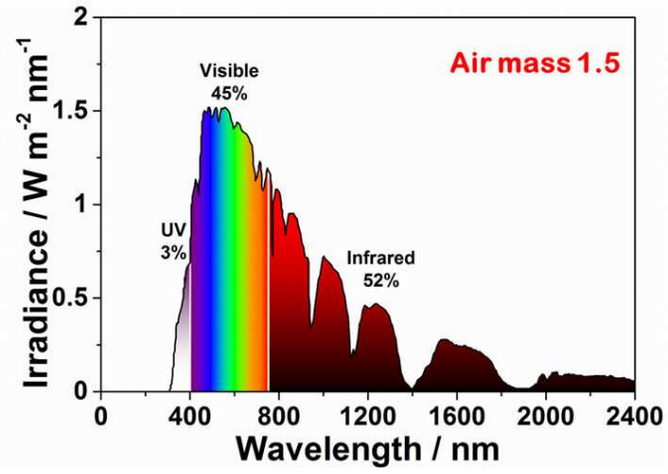

Figure 1. Solar spectrum (AM 1.5).

Conversely, $[Sn(acac)_2]Cl_2$ is adsorbed on TiO_2 via the ion exchange between H^+ and $[Sn(acac)_2]^{2+}$ ion (Eq. 2) [23]. In each case, the adsorption apparently obeys the Langmuir model. The saturated adsorption amount and the adsorption constant for the adsorption of various metal acetylacetonates on TiO_2 at 298 K are summarized in Table 1. The adsorption constants range from 10^2 to 10^4, indicating that they are strongly adsorbed on the TiO_2 surface by chemical bonds. Exceptionally, $Cr(acac)_3$ is not adsorbed because of its large ligand-field stabilization energy ($1.2\Delta_0$).

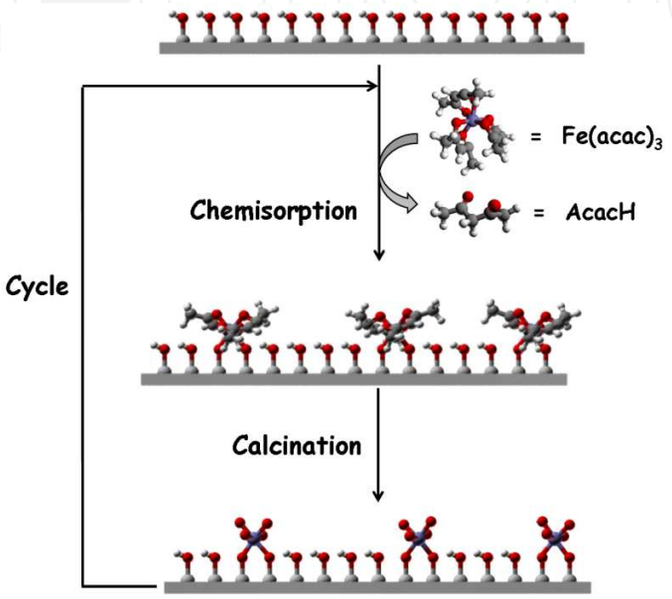

Sheme 2. Fe oxocomplex (Fe_2O_3) formation on the TiO_2 surface by the CCC technique.

TiO_2 (crystal form, specific surface area)	Precursor	Solvent	Saturated adsorption amount / ions nm^{-2}	Adsorption equilibrium constant / 10^3 mol^{-1} dm^3	Mechanism	Oxidation number of metal ion in oxide cluster [a]
ST-01 (A, 308 m^2 g^{-1})	$VO(acac)_2$	ethanol	0.18	1.67	ligand exchange	V^{5+} (V_2O_5)
P-25 (A-R, 50 m^2 g^{-1})	$Cr(acac)_3$	ethanol	0	0	—	—
P-25 (A-R, 50 m^2 g^{-1})	$Mn(acac)_3$	ethanol	1.65	0.17	ligand exchange	Mn^{3+} (Mn_2O_3)
P-25 (A-R, 50 m^2 g^{-1})	$Fe(acac)_3$	ethanol : n-hexane 3: 17 v/v	0.46	2.06	ligand exchange	Fe^{3+} (Fe_2O_3)
ST-01 (A, 308 m^2 g^{-1})			0.35	1.52		Fe^{3+} (Fe_2O_3)
ST-01 (A, 308 m^2 g^{-1})	$Co(acac)_2(H_2O)_2$	methanol	0.18	1.23	surface Ti-OH coordination	Co^{3+} (Co_2O_3)
P-25 (A-R, 50 m^2 g^{-1})	$Ni(acac)_2(H_2O)_2$	ethanol : n-hexane 3: 17 v/v	0.56	0.74	ligand exchange	Ni^{2+} (NiO)
P-25 (A-R, 50 m^2 g^{-1})	$Cu(acac)_2$	acetonitrile	0.54	1.34	surface Ti-OH coordination	Cu^{2+} (CuO)
A-100 (A, 8.1 m^2 g^{-1})	$[Sn(acac)_2]Cl_2$	ethanol	0.29	17.0	ion-exchange	Sn^{4+} (SnO_2)
MT-700B (R, 12.5 m^2 g^{-1})			0.10	46.0		Sn^{4+} (SnO_2)

Table 1. Adsorption properties of 3d metal acetylacetonates on TiO_2 at 298 K.

http://dx.doi.org/10.5772/62008

$$\left[\mathrm{Sn(acac)_2}\right]\mathrm{Cl_2} + 2\left(\mathrm{Ti_s\text{-}OH}\right) \rightarrow \mathrm{Sn(acac)_2\left(O\text{-}Ti_s\right)_2} + 2\mathrm{HCl} \quad (2)$$

In the second step, the oxidation of the acac ligands by heating the samples in air at 773 K yields iron oxides on the TiO_2 surface. Further, these procedures are repeated to control the Fe-loading amount. Chemical analysis confirmed that all the Fe was confirmed to be present only on the TiO_2 surface. The Fe-loading amount is expressed by the number of Fe ions per unit TiO_2 surface area (Γ/ions nm^{-2}).

3.2. Control of loading amount

A feature of the CCC technique is precise control of the loading amount of metal oxides. As an example, the manner in which the Fe-loading amount is controlled in the iron oxide/TiO_2 system is described. Figure 2A shows the relation between Γ and initial complex concentration: black, $Fe(acac)_3$ and blue, $Mn(acac)_3$. In each case, the Γ gradually increases with an increase in the initial concentration. Figure 2B shows plots of Γ versus CCC cycle number (N): black, $Fe(acac)_3]_0$ = 0.65 mmol dm^{-3} (black) and blue, $Mn(acac)_3]_0$ = 8 mmol dm^{-3}. The Γ further increases in proportional to N in both the systems. The linear Γ–N relation is also observed in the other metal oxide/TiO_2 systems. In this manner, the loading amount of metal oxides can be controlled in a wide range using the precursor complex concentration and the cycle number.

4. Structure of surface metal oxocomplexes

Another feature of the CCC technique is the formation of molecular-scale metal oxide species on TiO_2. Figure 3 shows transmission electron micrographs (TEMs) of iron oxide/TiO_2 with varying Γ. No particulate deposits are observed on the TiO_2 surface at $\Gamma < 1$ ions nm^{-2}. This fact suggests that iron oxides exist as molecular-scale iron oxide species on the TiO_2 surface.

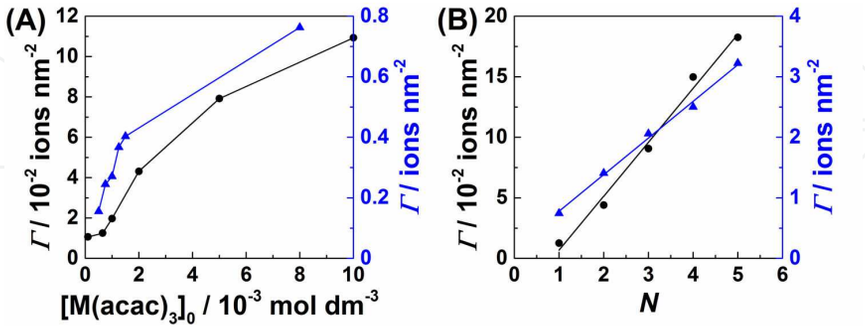

Figure 2. (A) Plots of Fe-loading amount (Γ/ions nm^{-2}) versus initial concentration of the complex ($[M(acac)_3]_0$): M = Fe (black) and M = Mn (blue). (B) Plots of Γ versus cycle number (N) at $Fe(acac)_3]_0$ = 0.65 mmol dm^{-3} (black) and $Mn(acac)_3]_0$ = 8 mmol dm^{-3} (blue).

To obtain the detailed structural information, Fe K-edge X-ray absorption fine-structure spectra were measured for the iron oxide/TiO_2 samples with varying Γ [24]. Figure 4A shows

X-ray absorption near-edge structure (XANES) spectra for the iron oxide/TiO_2 samples, and authentic Fe, Fe_3O_4, and α-Fe_2O_3 for comparison. The absorption edge of the iron oxide/TiO_2 sample is in agreement with that of α-Fe_2O_3, indicating the oxidation number of the iron to be +3 (Table 1). Figure 4B shows the Fourier transforms of the k^3-weighted X-ray absorption fine structure (EXAFS) for the iron oxide/TiO_2 samples. The peaks around 1.6 Å and 2.8 Å arise from the scattering from the nearest neighbor O and Fe, respectively. It is worth noting that the latter peak becomes very weak at $\Gamma \leq 0.5$. Evidently, the iron oxides exist as a mononuclear Fe oxocomplex on TiO_2 designated as Fe_2O_3/TiO_2 below.

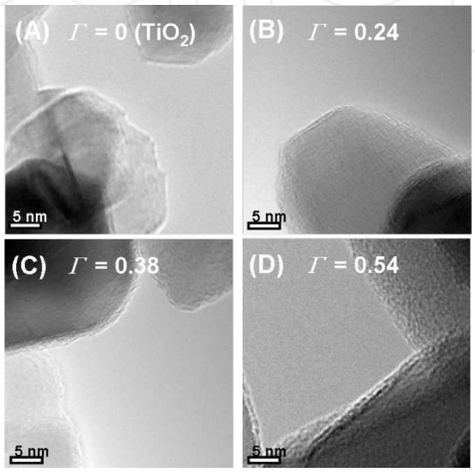

Figure 3. TEM images of Fe_2O_3/TiO_2 with varying Γ : (A) $\Gamma = 0$ (P-25); (B) $\Gamma = 0.23$, (C) $\Gamma = 0.38$, (D) $\Gamma = 0.54$.

In this manner, MOCs are formed on the TiO_2 surface in a highly dispersed state by the CCC technique, whereas the conventional impregnation method usually yields metal oxide NPs. As illustrated in Scheme 2, the molecular size of $Fe(acac)_3$ (~0.5 nm^2 $complex^{-1}$) is much larger than the reciprocal number density of the Ti-OH groups on the TiO_2 surface (~0.1 nm^2 $group^{-1}$) [25]. In the first step of the CCC process, $Fe(acac)_3$ complexes are chemisorbed isolatedly each other owing to the bulky acac-ligands. Also, the strong bond between the complexes and the TiO_2 surface suppresses the aggregation of the oxocomplexes during the second step. Consequently, mononuclear MOCs can be formed on the TiO_2 surface.

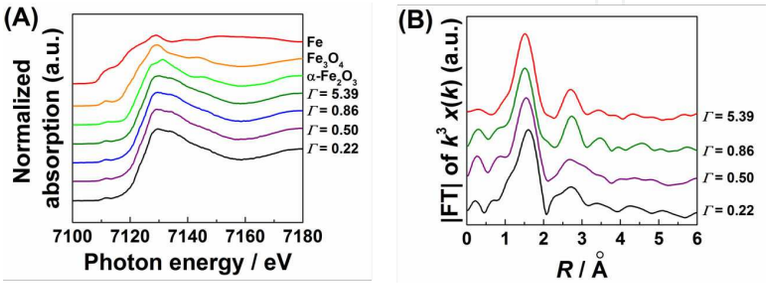

Figure 4. XANES and EXAFS spectra. (A) XANES spectra for Fe, Fe_3O_4, α-Fe_2O_3, and Fe_2O_3/TiO_2 with varying Γ. (B) Fourier transforms of the k^3-weighted EXAFS spectra for Fe_2O_3/TiO_2. The figures were taken from Ref. 24.

http://dx.doi.org/10.5772/62008

5. Characteristics of metal oxocomplex–surface-modified TiO_2

5.1. Optical property

The optical property is a fundamental factor affecting the photocatalytic activity. Figure 5 shows UV–visible absorption spectra for Fe oxocomplex–surface-modified mesoporous TiO_2 nanocrystalline films (Fe_2O_3/mp-TiO_2) with varying Γ. Impregnation samples usually have absorption approximately 470 nm in addition to absorption at 410 nm [16,17,26,27]. The former and latter absorptions can be attributed to the d–d transition and electronic transition from Fe^{3+} levels to the CB of TiO_2, respectively [28]. A strong d–d absorption is also observed for a heavy-loading CCC sample (Fe_2O_3(Γ = 5.5)/mp-TiO_2). In contrast, the absorption spectra of Fe_2O_3($\Gamma \leq 2.1$)/mp-TiO_2 apparently show a marked bandgap narrowing from 3.3 to 2.85 eV with an increase in Γ, whereas the d–d transition absorption is very weak [24]. Similar spectra were previously observed for TiO_2 doped with Cr [12] and N [13] prepared by ion implantation and magnetron sputtering. The weak d–d transition absorption is a common feature for the CCC samples including Co_2O_3/TiO_2 [29], NiO/TiO_2 [30,31], and CuO/TiO_2 [32]. Clearly, the unique optical properties of the CCC samples originate from the highly dispersed MOCs on the TiO_2 surface.

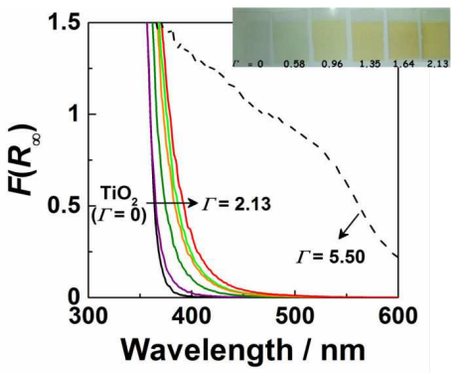

Figure 5. UV–Vis absorption spectra of Fe_2O_3/mp-TiO_2 prepared by the CCC technique.

5.2. Fine-tuning of band energy

The VB maximum determines the oxidation ability of the holes, and thus is a key factor for the decomposition of organic pollutants by semiconductor photocatalysts. The VB maximum level can be estimated from the VB-X-ray photoelectron spectroscopy (XPS) [24]. Since the VB maximum of TiO_2 is almost independent of its crystal form and size, the VB maximum of MOC-modified TiO_2 can be compared with respect to that of unmodified TiO_2. Figure 6 shows the VB-XPS spectra for Fe_2O_3/TiO_2 with varying Γ. The emission from the O 2*p*–VB extends from 2 to 9 eV. As a result of the surface modification, the top of VB rises, whereas the bottom remains invariant. Figure 6B compares the energy shift in the VB maximum level with respect to that of unmodified TiO_2 (ΔE_{VBM}) as a function of Γ for the Fe_2O_3/TiO_2, Co_2O_3/TiO_2, NiO/TiO_2, and SnO_2/TiO_2 systems. Interestingly, the ΔE_{VBM} for the MOC-modified TiO_2, except SnO_2/TiO_2,

goes up with an increase in Γ, which means that the oxidation ability of the VB holes can be tuned by Γ. This is the most unique and important feature of the TiO_2 modification with MOCs using the CCC technique.

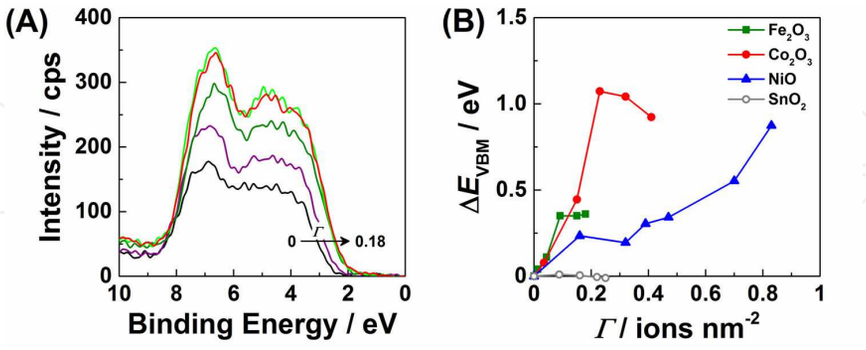

Figure 6. (A) VB-XPS spectra for Fe_2O_3/TiO_2 with varying Γ. (B) Energy shift in the VB maximum level (ΔE_{VBM}) as a function Γ for various MOCs/TiO_2. The figure (A) was taken from ref. 35.

These results were further simulated by the density functional theory (DFT) calculations [7]. In the DFT-optimized structure for a model Fe_2O_3 cluster-adsorbed TiO_2 system, plural Fe–O–Ti interfacial bonds were observed. The PEDOS (projected electronic density of states) plots showed that states from the adsorbed Fe_2O_3 clusters lie above the VB of TiO_2, that is, the iron oxide-derived states make it to the top of the VB. This changes the nature of the VB edge that moves the top of the VB to higher energy. The offsets between the TiO_2 VB edge and the iron oxide states around the VB are ~0.3 eV for Fe_2O_3-modified TiO_2, which is comparable with the experimental value. The effective mixing between the surface Fe_2O_3 levels and O 2*p* through the Ti_s–O–Fe interfacial bond is considered as yielding a d-band overlapping the VB of TiO_2. Thus, the excitation of Fe_2O_3/TiO_2 by the visible light with wavelength below 500 nm can induce the interfacial electron transfer from the surface d-band to the CB of TiO_2.

Conversely, the information about empty levels can be obtained by photoluminescence spectroscopy. TiO_2(ST-01) has a broad emission band centered at 538 nm (E_1) [22]. The E_1 signal intensity remarkably weakens with heating ST-01 at 773 K for 1 h in air. This PL band is assignable to the emission from the surface oxygen vacancy levels of anatase TiO_2 [33]. On modifying ST-01 with the Fe oxocomplexes, the intensity further decreases to disappear at $\Gamma > 0.044$ ions nm^{-2}, while a new emission appears at 423 nm (E_2). The E_2 signal can be attributed to the emissions from extrinsic levels. These findings strongly suggest that the excited electrons in the CB of TiO_2 are transferred to the empty surface Fe oxocomplex levels with the energy distributed around 0.27 V below the CB of TiO_2.

5.3. Electrocatalytic activity for oxygen reduction reaction

As stated above, the ORR is frequently the key process in the TiO_2-photocatalyzed reactions as well as low-temperature polymer electrolyte membrane fuel cells (PEMFCs) [34,35]. Figure 7 shows dark current (*I*)–potential (*E*) curves of the mp-TiO_2 film-coated F-doped tin oxide (FTO) electrodes (mp-TiO_2/FTO) with and without the surface modification by Fe oxocom-

http://dx.doi.org/10.5772/62008

plexes. In the absence of O_2, a small current due to water reduction is observed regardless of the surface modification. In the presence of O_2, the current for ORR markedly increases with the surface modification (Fe_2O_3/mp-TiO_2/FTO), whereas it remains weak without O_2. In this manner, the surface Fe oxocomplex has an electrocatalytic activity for the ORR, and a similar ORR-promoting effect is also observed for the NiO/TiO_2 [30] and Co_2O_3/TiO_2 [29] systems. This is also the unique feature of the MOC/TiO_2 systems.

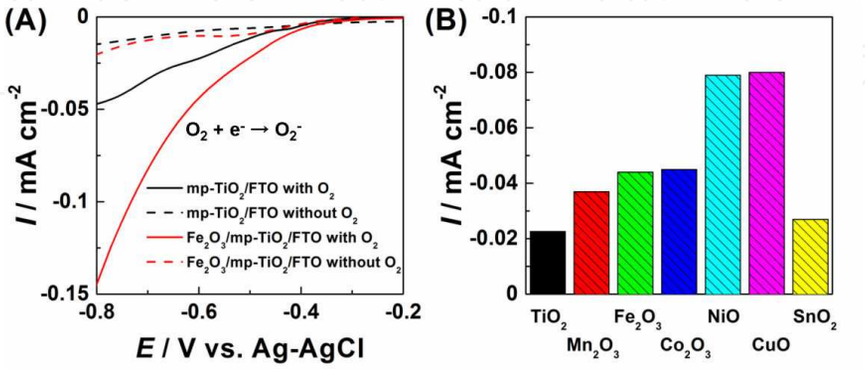

Figure 7. (A) Dark current (I)–potential (E) curves for the Fe_2O_3/mp-TiO_2/FTO electrodes. (B) Comparison of the electrocatalytic activity of the MOC/mp-TiO_2/FTO electrodes for the ORR.

6. Photocatalytic activity

Acetaldehyde is a toxic volatile organic compound (VOC), while 2-naphthol is widely used as the starting material of azo dyes. Both of them are optically transparent in the visible region, and then, acetaldehyde and 2-naphthol were used as model air and water pollutants, respectively. The relative photocatalytic activities of various MOCs/TiO_2 were evaluated with respect to that of highly active commercial TiO_2 particles with a crystal form of anatase (ST-01, Ishihara Sangyo Co.). The photocatalytic degradation of 2-naphthol and acetaldehyde apparently follows the first-order rate law, and the rate constants for irradiation of UV light ($330 < \lambda < 400$ nm, k_{UV}) and visible light ($\lambda > 400$ nm, k_{vis}) were used as the indicators for the photocatalytic activities. Figure 8 shows the k_{vis} and k_{UV} of Fe_2O_3/TiO_2 for the degradations of 2-naphthol (A) and acetaldehyde (B) as a function of Γ. Surprisingly, the surface modification of TiO_2 by the Fe-oxocomplex gives rise to a high level of visible-light activity and a concomitant increase in the UV-light activity of anatase TiO_2 [24]. Each plot exhibits a volcano-shaped curve, which is a general feature in the activity-Γ plots for the MOC/TiO_2 systems. By using an atomic layer deposition technique, Libera et al. have recently prepared Fe(III) oxospecies–surface-modified TiO_2 showing a reactivity for the decoloration of methylene blue under visible-light irradiation [18].

Particulate systems have high photocatalytic activity due to the large surface area, but needs the troublesome separation of the particles from purified water. Oppositely, in supported films, the photocatalytic activity is generally much lower due to the smaller surface area,

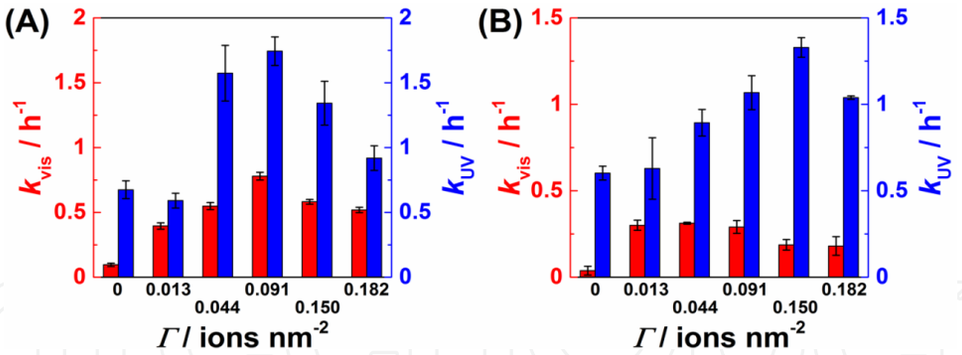

Figure 8. (A) UV-light activity (k_{UV}, blue) and visible-light activity (k_{vis}, red) of Fe_2O_3/TiO_2(ST-01) for the liquid-phase decomposition of 2-NAP as a function of Γ. (B) UV-light activity (k_{UV}, blue) and visible-light activity (k_{vis}, red) of Fe_2O_3/TiO_2(ST-01) for the gas-phase decomposition of CH_3CHO as a function of Γ.

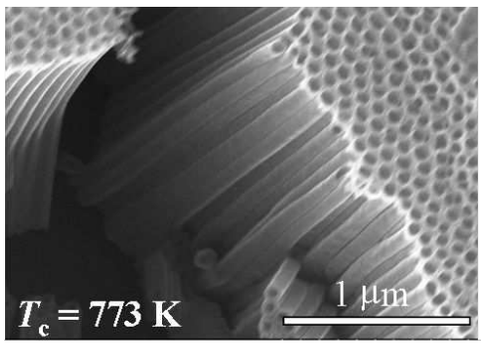

Figure 9. TiO_2 NTA parepared by a two-step anodization of Ti plate (first anodization 40 V, 0.5 h/second anodization 40 V-1 h/heating temperature, T_c = 773 K). The figure was taken from Ref. 35.

while the separation process is unnecessary. TiO_2 nanotube array (NTA) has the advantages of the particulate and film systems is promising. Figure 9 shows TEM image for TiO_2 NTA prepared by two-step anodization. The application of the CCC technique to the TiO_2 NTA led to a high visible-light activity for 2-naphthol degradation comparable with that of the particulate system [36].

Figure 10 compares the relative visible-light activity (k_{vis}) and UV-light activity (k_{UV}) of 3d MOCs/TiO_2(ST-01) with respect to the activities of unmodified TiO_2(ST-01) (k_{vis}^0 and k_{UV}^0) for the 2-naphthol degradation under the same conditions. Each Γ shows the optimum value for visible-light activity in each MOC/TiO_2 system. Among MOCs, the surface modification by Fe_2O_3 [24], Co_2O_3 [25], and NiO [30] is effective in the visible-light activation. Particularly, the Co_2O_3/TiO_2 system exhibits a very high level of visible-light activity [29]. The activity is on the order of Co_2O_3 > Fe_2O_3 > NiO > CuO > V_2O_5 ≈ Mn_2O_3 > SnO_2 ≈ unmodified TiO_2. However, the surface modification with Fe_2O_3, NiO, and Co_2O_3 by the CCC technique can endow anatase TiO_2 with high levels of visible-light activity, with the high UV-light activity further increased (Fe_2O_3) or maintained (Co_2O_3, NiO). Although the effect of the surface modification by SnO_2 was small for anatase, a significant increase in the UV-light activity was induced for rutile [37]. Interestingly, Boppana and Lobo have

http://dx.doi.org/10.5772/62008

recently reported that loading of SnO_x clusters on $ZnGa_2O_4$ by the impregnation method causes visible-light activity for the decomposition of p-cresol [38]. Besides metal oxides, the surface modification of TiO_2 with halogeno complexes of rhodium(III) and platinum(IV) on the TiO_2 surface is known to induce visible-light activity [39,40].

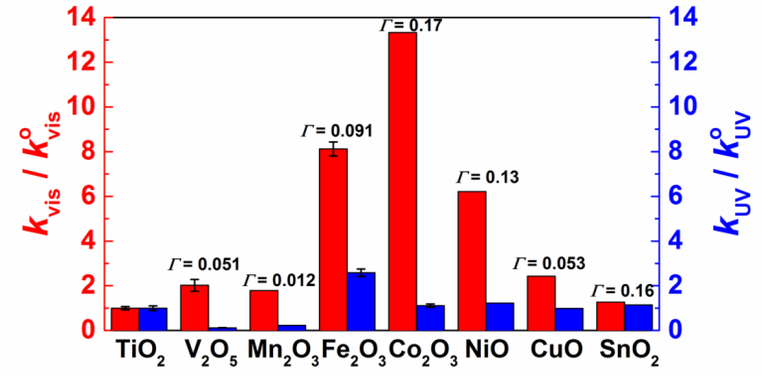

Figure 10. Comparison of the visible-light activities (k_{vis}) and UV-light activities (k_{UV}) of MOCs/TiO_2(ST-01) with respect to those of unmodified TiO_2 for the 2-naphthol degradation under the same conditions.

The degradation of formic acid was further carried out in the aqueous phase with Co_2O_3/TiO_2 at 298 K under visible-light irradiation. The Co_2O_3 surface modification greatly enhanced the decomposition of formic acid to CO_2. The visible-light activity reached a maximum at Γ = 0.17 with the conversion to CO_2 reaching ~100% within 5 h [29] (Eq. 3).

$$HCOOH+1/2O_2 \xrightarrow[h\nu(\lambda>400nm)]{CO_2O_3/TiO_2} CO_2+H_2O \quad (3)$$

Also, prolonging irradiation decomposed 2-naphthol to CO_2, but the conversion was only ~6% at 96 h. The decomposition of 2-naphthol to CO_2 would proceed stepwise via oxidative cleavage of the naphthalene ring.

On the basis of the energy band diagram, the action mechanism of MOCs in the TiO_2 photocatalysis can be explained. In the nanoscale Fe_2O_3–TiO_2 coupling system, Fe_2O_3 NP with a band gap of 2.2 eV is excited by the visible-light irradiation. However, the potential of the CB electrons is more positive than the TiO_2 CB minimum of TiO_2 (−0.48 V) and the standard redox potential of O_2 ($E^0(O_2/O_2^-)$ = −0.284 V). Thus, the electron transfer from the CB electrons of Fe_2O_3 to neither TiO_2 nor O_2 can occur. Consequently, nano-coupling does not show visible-light activity [41].

Scheme 3 illustrates the surface modification effects of the Fe oxocomplex on the TiO_2 photocatalytic decomposition of organic pollutants. In this case, the surface modification raises the VB maximum with the CB minimum unchanged, due to the effective electronic coupling through the Fe–O–Ti interfacial bonds (Effect 1). The resulting decrease in the band gap shifts the light absorption to the visible region (Effect 2). The visible-light absorption triggers electronic excitation from the highest-energy oxocomplex-derived VB states to the empty CB

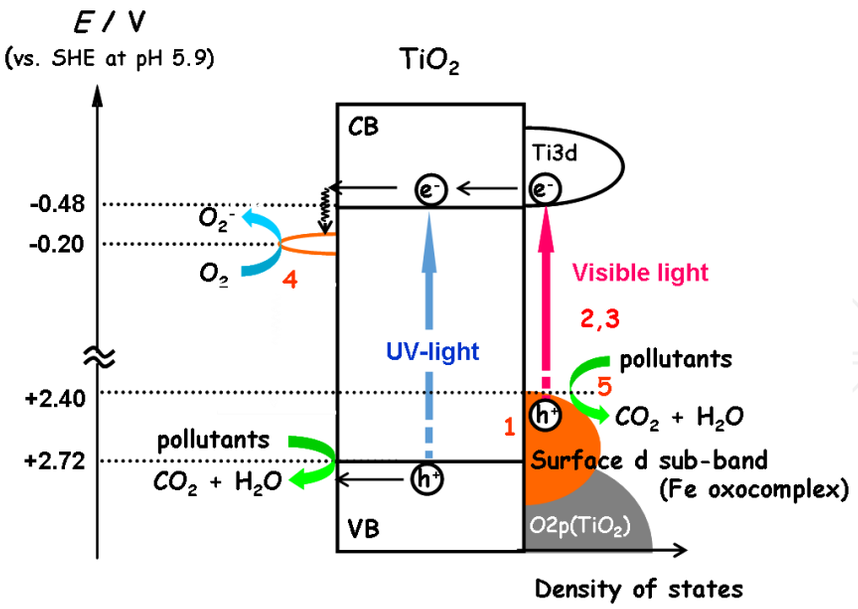

Sheme 3. Surface modification effects of the Fe oxocomplex on the TiO_2-photocatalyzed decomposition of organic pollutants. The levels around −0.2 V show the vacant Fe oxocomplex.

of TiO_2 in order to generate charge carriers. This surface-to-bulk interfacial electron transfer enhances charge separation (Effect 3). The surface modification permits the electron transfer from the CB of TiO_2 to shallow vacant surface oxocomplex levels, which distribute around ca. −0.2 V [22]. The formation of O_2^- radicals was confirmed by chemiluminescence photometry in the Cu^{2+}-grafted TiO_2 system under visible-light irradiation [42]. In this cathodic process, the electrons efficiently reduce adsorbed O_2 with the aid of the electrocatalytic activity of the surface-adsorbed oxocomplex (Effect 4). This effect should also contribute to the increase in the UV-light activity. In the anodic process, the holes generated in the VB could take part in the oxidation process without diffusion (Effect 5) [15]. Consequently, Fe_2O_3/TiO_2 as well as NiO/TiO_2 and Co_2O_3/TiO_2 satisfy the three requirements of the "solar environmental catalyst."

7. Conclusions and future prospect

The surface of TiO_2 can be modified by oxocomplexes of the first transition metals (MOCs/TiO_2) with the loading amount precisely controlled by using the CCC technique. Among the MOCs/TiO_2, Fe_2O_3-, Co_2O_3- and NiO-surface-modified TiO_2 possess unique physicochemical properties such as strong visible-light absorption and the excellent reduction ability of O_2. Spectroscopic experiments and first-principles DFT simulation have revealed that the surface modification with the MOCs raises the VB maximum of TiO_2 due to the formation of plural metal–O–Ti interfacial bonds. Surface-to-bulk and/or bulk-to-surface interfacial electron transfer induced by visible-light absorption enhances charge separation. This novel coupling system consisting of MOCs and TiO_2 would be promising as the "solar environmental catalyst."

The standard potentials of multiple-electron ORRs ($E^0(O_2/H_2O_2)$ = +0.695 V and $E^0(O_2/H_2O)$ = +1.229 V versus SHE) are much more positive than that of one-electron ORR. Therefore, the hybridization of appropriate electrocatalysts for the multiple-electron ORR can impart visible-light activity to many metal oxide semiconductors with E_g < 3 eV. The effectiveness of this approach has recently been verified in the Pt NP-WO_3 (E_g = 2.7 eV) [43] and $Cu(acac)_2$-$BiVO_4$ (E_g = 2.4 eV) hybrid systems [44], where Pt NP and O_2-bridged Cu complex work as excellent electrocatalysts for multiple ORRs, respectively.

As a future subject, we further suggest the importance of the effective use of the infrared ray occupying 52% of the solar energy for the catalytic reactions (Figure 1). For example, Co_2O_3/TiO_2 exhibits high levels of photocatalytic and thermocatalytic activities [29], whereas Mn_2O_3/TiO_2 exhibits a high thermocatalytic activity for the oxidation of organic compounds [45]. Further, MOCs/TiO_2 with the VB maximum level (or the oxidizing ability of the VB holes) fine-tuned by the loading amount may open up the application of MOCs/TiO_2 to "green" and selective chemical transformations [46–48].

Acknowledgements

A series of studies on metal oxocomplex–surface-modified TiO_2 have been performed in collaboration with Dr. Michael Nolan and Dr. Anna Iwaszuk (Tyndall National Institute, University College Cork). The authors are sincerely grateful for their very useful DFT simulations. Also, the authors acknowledge Dr. M. Fujishima (Kinki University) for a helpful discussion, and T. Hattori, S. Okuoka, and Y. Sumida (Nippon Shokubai Co.) for EXAFS measurements and a valuable discussion. Ishihara Sangyo Co. gifted us with ST-01, and K. Fujiwara aided us in the collection and arrangement of the materials. H.T. acknowledges the support from the Ministry of Education, Science, Sport, and Culture, Japan, through a Grant-in-Aid for Scientific Research (C) No. 24550239, No. 15K05654, MEXT-Supported Program for the Strategic Research Foundation at Private Universities, and Nippon Sheet Glass Foundation for Materials Science and Engineering, and by Sumitomo Foundation.

Author details

Hiroaki Tada[1*] and Qiliang Jin[2]

*Address all correspondence to: h-tada@apch.kindai.ac.jp

1 Department of Applied Chemistry, School of Science and Engineering, Kinki University, Kowakae, Higashi-Osaka, Osaka, Japan

2 R&D Placement Business Division, WORLD INTEC CO., Sakae, Naka-ku, Nagoya, Aichi, Japan

References

[1] Fujishima A, Zhang X, Tryk D A: TiO_2 photocatalysis and related surface phenomena. Surf. Sci. Rep. 2008; 63: 515–582. DOI: j.surfrep.2008.10.001

[2] Hashimoto K, Irie H, Fujishima A: TiO_2 photocatalysis: A historical overview and future prospects. Jpn. J. Appl. Phys. 2005; 44: 8269–8285.

[3] Hoffmann M R, Martin S T, Choi W, Bahnemann D W: Environmental applications of semiconductor photocatalysis. Chem. Rev. 1995; 95: 69–96. DOI: 10.1021/cr00033a004

[4] A. Y. Ahmed, T. A. Kandiel, T. Oekermann, D. Bahnemann: Photocatalytic activities of different well-defined single crystal TiO_2 surfaces: Anatase versus rutile. J. Phys. Chem. Lett. 2011; 2: 2461–2465. DOI: 10.1021/jz201156b

[5] Kawahara T, Konishi Y, Tada H, Tohge N, Nishii J, Ito S: A patterned TiO_2(anatase)/TiO_2(rutile) bilayer-type photocatalyst: Effect of the anatase/rutile junction on the photocatalytic activity. Angew. Chem. Int. Ed. 2002; 41: 2811–2813. DOI: 10.1002/1521-3757(20020802)114:15<2935:: AID-ANGE2935>3.0.CO;2-6

[6] Kisch H: Semiconductor photocatalysis–mechanistic and synthetic aspects. Angew. Chem. Int. Ed. 2013; 52: 812–847. DOI: 10.1002/anie.201201200

[7] Nolan M, Iwaszuk A, Tada H: Molecular metal oxide cluster-surface modified titanium(IV) dioxide photocatalysts. Aust. J. Chem. 2012; 65: 624–632.

[8] Asahi R, Morikawa T, Ohwaki T, Aoki K, Taga Y: Visible-light photocatalysis in nitrogen-doped titanium oxides. Science 2001; 293: 269–271. DOI: 10.1126/science. 1061051

[9] Khan S U M, Al-Shahry M, Ingler Jr. W B: Efficient photochemical water splitting by a chemically modified n-TiO_2. Science 2002; 297: 2243–2245. DOI: 10.1126/science. 1075035

[10] Serpone N: Is the band gap of pristine TiO_2 narrowed by anion- and cation-doping of titanium dioxide in second-generation photocatalysts? J. Phys. Chem. B 2006; 110: 24287–24293. DOI: 10.1021/jp065659r

[11] Zhang H, Chen G, Bahnemann D W: Photoelectrocatalytic materials for environmental applications. J. Mater. Chem. 2009; 19: 5089–5121. DOI: 10.1039/B821991E

[12] Anpo M, Takeuchi M: The design and development of highly reactive titanium oxide photocatalysts operating under visible light irradiation. J. Catal. 2003; 216: 505–516. DOI: 10.1016/S0021-9517(02)00104-5

[13] Kitano M, Funatsu K, Matsuoka M, Ueshima M, Anpo M: Preparation of nitrogen-substituted TiO_2 thin film photocatalysts by the radio frequency magnetron sputtering deposition method and their photocatalytic reactivity under visible light irradiation. J. Phys. Chem. B 2006; 110: 25266–25272. DOI: 10.1021/jp064893e

[14] Liu G, Wang L, Yang H G, Cheng H-M, Lu G Q: Titania-based photocatalysts-crystal growth, doping and heterostructuring. J. Mater. Chem. 2010; 20: 831–843. DOI: 10.1039/B909930A

[15] Irie H, Shibanuma T, Kamiya K, Miura S, Yokoyama T, Hashimoto K: Characterization of Cr(III)-grafted TiO_2 for photocatalytic reaction under visible light. Appl. Catal. B. 2010; 96: 142–148. DOI: 10.1016/j.apcatb.2010.02.011

[16] Murakami N, Chiyoya T, Tsubota T, Ohno T: Switching redox site of photocatalytic reaction on titanium(IV) oxide particles modified with transition-metal ion controlled by irradiation wavelength. Appl. Catal. A. 2008; 348: 148–152. DOI: 10.1016/j.apcata.2008.06.040

[17] Yu H, Irie H, Shimodaira Y, Hosogi Y, Kuroda Y, Miyauchi M, Hashimoto K: J. Phys. Chem. C 2010; 114: 16481–16487. DOI: 10.1021/jp1071956

[18] Libera J A, Elam J W, Sather N F, Rajh T M, Dimitrijevic N M: Iron(III)-oxo centers on TiO_2 for visible-light photocatalysis. Chem. Mater. 2010; 22: 409–413. DOI: 10.1021/cm902825c

[19] Irie H, Miura S, Kamiya K, Hashimoto K: Efficient visible light-sensitive photocatalysts: Grafting Cu(II) ions onto TiO_2 and WO_3 photocatalysts. Chem. Phys. Lett. 2008; 457: 202–205. DOI: 10.1016/j.cplett.2008.04.006

[20] Tada H: Encyclopedia of Surface and Colloid Science. Ed. Hubbard A T, New York: Marcel Dekker, 2002. ISBN: 0-8247-0633-1

[21] Wang C-M, Heller A, Gerischer H: Palladium catalysis of O_2 reduction by electrons accumulated on TiO_2 particles during photoassisted oxidation of organic compounds. J. Am. Chem. Soc. 1992; 114: 5230–5234. DOI: 10.1021/ja00039a039

[22] Jin Q, Fujishima M, Tada H: Visible-light-active iron oxide-modified anatase titanium(IV) dioxide. J. Phys. Chem C 2011; 115: 6478–6483. DOI: 10.1021/jp201131t

[23] Fujishima M, Jin Q, Yamamoto H, Tada H, Nolan M: Tin oxide-surface modified anatase titanium(IV) dioxide with enhanced UV-light photocatalytic activity. Phys. Chem. Chem. Phys. 2012; 14: 705–711. DOI: 10.1039/C1CP22708D

[24] Tada H, Jin Q, Nishijima H, Yamamoto H, Fujishima M, Okuoka S-i, Hattori T, Sumida Y, Kobayashi H: Titanium(IV) dioxide surface-modified with iron oxide as a visible light photocatalyst. Angew. Chem. Int. Ed. 2011; 50: 3501–3505. DOI: 10.1002/anie.201007869

[25] Nosaka Y, Nosaka A. Nyumon: Hikarisyokubai (Introduction to Photocatalyst). Tokyo: Tokyo-Tosho; 2004, 68 p. ISBN: 4-489-00684-5 C3043

[26] Navio J A, Colon G, Litter M I, Bianco G N: Synthesis, characterization and photocatalytic properties of iron-doped titania semiconductors prepared from TiO_2 and

iron(III) acetylacetonate. J. Mol. Catal. A: Chem. 1996; 106: 267–276. DOI: 10.1016/1381-1169(95)00264-2

[27] Wang C-Y, Bahnemann D W, Dohrmann J K: A novel preparation of iron-doped TiO_2 nanoparticles with enhanced photocatalytic activity. Chem. Commun. 2000; 1539–1540. DOI: 10.1039/B002988M

[28] Serpone N, Lawless D, Disdier J, Hermann J-M: Spectroscopic, photoconductivity, and photocatalytic studies of TiO_2 colloids: Naked and with the lattice doped with Cr^{3+}, Fe^{3+}, and V^{5+} cations. Langmuir 1994; 10: 643–652. DOI: 10.1021/la00015a010

[29] Jin Q, Yamamoto H, Yamamoto K, Fujishima M, Tada H: Simultaneous induction of high level thermal and visible-light catalytic activities to titanium(IV) oxide by surface modification with cobalt(III) oxide clusters. Phys. Chem. Chem. Phys. 2013; 15: 20313–20319. DOI: 10.1039/C3CP54304H

[30] Jin Q, Ikeda T, Fujishima M, Tada H: Nickel(II) oxide surface-modified titanium(IV) dioxide as a visible-light-active photocatalyst. Chem. Commun. 2011; 47: 8814–8816. DOI: 10.1039/C1CC13096J

[31] Iwaszuk A, Nolan M, Jin Q, Fujishima M, Tada H: Origin of the visible-light response of nickel(II) oxide cluster surface modified titanium(IV) dioxide. J. Phys. Chem. C 2013; 117: 2709–2718. DOI: 10.1021/jp306793r

[32] Jin Q, Fujishima M, Iwaszuk A, Nolan M, Tada H: Loading effect in copper(II) oxide cluster-surface-modified titanium(IV) oxide on visible- and UV-light activities. J. Phys. Chem. C 2013; 117: 23848–23857. DOI: 10.1021/jp4085525

[33] Shi J, Chen J, Feng Z, Chen T, Lian Y, Wang X, Li C: Photoluminescence characteristics of TiO_2 and their relationship to the photoassisted reaction of water/methanol mixture. J. Phys. Chem. 2007; 111: 693–699. DOI: 10.1021/jp065744z

[34] Gewirth A A, Thorum M S: Electroreduction of dioxygen for fuel-cell applications: Materials and challenges. Inorg. Chem. 2010; 49: 3557–3566. DOI: 10.1021/ic9022486

[35] Fermández J L, Walsh D A, Bard A J: Thermodynamic guidelines for the design of bimetallic catalysts for oxygen electroreduction and rapid screening by scanning electrochemical microscopy. M-co (M: Pd, Ag, Au). J. Am. Chem. Soc. 2005; 127: 357–365. DOI: 10.1021/ja0449729

[36] Muramatsu Y, Jin Q, Fujishima M, Tada H: Visible-light-activation of TiO_2 nanotube array by the molecular iron oxide surface modification. Appl. Catal. B: Environ. 2012; 119–120: 74–80. DOI: 10.1016/j.apcatb.2012.02.012

[37] Jin Q, Fujishima M, Nolan M, Iwaszuk A, Tada H: Photocatalytic activities of tin(IV) oxide surface-modified titanium(IV) dioxide show a strong sensitivity to the TiO_2 crystal form. J. Phys. Chem. C 2012; 116: 12621–12626. DOI: 10.1021/jp302493f

[38] Boppana V B R, Lobo R F: SnOx-$ZnGa_2O_4$ photocatalysts with enhanced visible light activity. ACS Catal. 2011; 1: 923–928. DOI: 10.1021/cs200137h

[39] Kisch H: Semiconductor photocatalysis-mechanistic and synthetic aspects. Angew. Chem. Int. Ed. 2013; 52: 812–847. DOI: 10.1002/anie.201201200

[40] Kitano S, Murakami N, Ohno T, Mitani Y, Nosaka Y, Asakura H, Teramura K, Tanakia T,

[41] Tada H, Hashimoto K, Kominami H: Bifunctionality of Rh^{3+} modifier on TiO_2 and working mechanism of Rh^{3+}/TiO_2 photocatalyst under irradiation of visible light. J. Phys. Chem. C 2013; 117: 11008–11016. DOI: 10.1021/jp311801e

[42] Lin X, Li D-Z, Wu Q-P, Fu X-Z, Wang X-X: Chem. Photocatalytic activity and mechanism of heterojunction thin films. J. Chin. Univ. 2005; 26: 727–730.

[43] Nosaka Y, Takahashi S, Sakamoto H, Nosaka A: Reaction mechanism of Cu(II)-grafted visible-light responsive TiO_2 and WO_3 photocatalysts studied by means of ESR spectroscopy and chemiluminescence photometry. J. Phys. Chem. C 2011; 115: 21283–21290. DOI: 10.1021/jp2070634

[44] Abe R, Takami H, Murakami N, Ohtani B: Pristine simple oxides as visible light driven photocatalysts: Highly efficient decomposition of organic compounds over platinum-loaded tungsten oxide. J. Am. Chem. Soc. 2008; 130: 7780–7781. DOI: 10.1021/ja800835q

[45] Naya S, Niwa T, Negishi R, Kobayashi H, Tada H: Multi-electron oxygen reduction by a hybrid visible-light-photocatalyst consisting of metal-oxide semiconductor and self-assembled biomimetic complex. Angew. Chem. Int. Ed. 2014; 53: 13894–13897. DOI: 10.1002/anie.201408352

[46] Jin Q, Arimoto H, Fujishima M, Tada H: Manganese oxide-surface modified titanium(IV) dioxide as environmental catalyst. Catalysts 2013; 3: 444–454. DOI: 10.3390/catal3020444

[47] Ide Y, Hattori H, Ogo S, Sadakane M, Sano T: Highly efficient and selective sunlight-induced photocatalytic oxidation of cyclohexane on an eco-catalyst under a CO_2 atmosphere. Green Chem. 2012; 14: 1264–1267. DOI: 10.1039/C2GC16594E

[48] Higasihmoto S, Shirai R, Osano Y, Azuma M, Ohue H, Sakata Y, Kobayashi H: Influence of metal ions on the photocatalytic activity: Selective oxidation of benzyl alcohol on iron (III) ion-modified TiO_2 using visible light. J. Catal. 2014; 311: 137–143. DOI: 10.1016/j.jca.2013.11.013

[49] Tang J, Grampp G, Liu Y, Wang, B-X, Tao F-F, Wang L-J, Liang X-Z, Xiao H-Q, Shen, Y-M: Visible light mediated cyclization of tertiary anilines with maleimides using nickel(II) oxide surface-modified titanium dioxide catalyst. J. Org. Chem. 2015; 80: 2724–2732. DOI: 10.1021/jo502901h

IntechOpen